X-ray-absorption spectroscopy of a Nd^{3+}-exchanged β''-alumina crystal

F. Rocca
Centro di Fisica degli Stati Aggregati ed Impianto Ionico del Consiglio Nazionale delle Ricerche, I-38050 Povo, Trento, Italy

A. Kuzmin and J. Purans
Institute of Solid State Physics, University of Latvia, LV-1063 Riga, Latvia

G. Mariotto
Dipartimento di Fisica, Università di Trento, I-38050 Povo, Trento, Italy
(Received 23 November 1993; revised manuscript received 22 April 1994)

We present an x-ray-absorption spectroscopy study of the electronic and crystallographic structure around the Nd^{3+} ions in 60% Nd-exchanged sodium β''-alumina crystal. Using a multishell best-fit analysis procedure, we reconstructed the Nd^{3+} local environment and compared it with existing structural models. We found that neodymium ions are mainly located near the mO(9d) sites of the conduction region; they are strongly bonded to two O(5) oxygens which are located in the same plane and shifted from their ideal crystallographic positions in sodium β''-alumina crystal. In particular, with respect to crystallographic parameters of sodium β''-alumina, the Nd-O(5) distance is shortened by 0.36 Å, while the Nd-Al(6c) is slightly increased by 0.13 Å. Comparative analysis of Debye-Waller factors obtained for different coordination shells shows evidence of correlation in the vibrational motion of neodymium with the O(5) oxygens and with the Al(6c) aluminums.

I. INTRODUCTION

Sodium β''-alumina is an hexagonal aluminate, with typical composition $Na_{1.67}Mg_{0.67}Al_{10.33}O_{17}$, which shows a unique ability to incorporate, by ion exchange reactions, a variety of lanthanide ions in the conduction region between two spinel blocks.[1] The exchanged compositions exhibit very interesting optical properties, which make β'' alumina a very promising candidate for optoelectronic applications.[2] Recently, there has been a noticeable interest in Nd^{3+}-exchanged β''-alumina crystals, especially after the lasing effect has been observed.[3]

A variety of structural methods [x-ray diffraction[4] (XRD) and transmission electron microscopy[5] (TEM)], several spectroscopic techniques [optical absorption,[6–8] electron paramagnetic resonance (EPR),[7] and x-ray absorption[9–11]], and molecular-dynamics simulations[11] were previously utilized to probe the local enviroment of Nd^{3+} ions at different levels of ion exchange in the disordered lattice of β''-alumina crystals.

Room-temperature XRD studies, carried out on single crystals, have shown that Nd^{3+} ions in highly exchanged β'' alumina exhibit a strong preference (95%) for mid-oxygen-site mO(9d) occupancy.[4] Here they are coordinated to two closely located oxygen atoms O(5) in the conduction region ($R \approx 2.46$ Å) and to six oxygen atoms in the spinel blocks ($R \approx 2.70$ Å). The remaining 5% of neodymium ions is suggested to lie in the Beever-Ross site BR(6c). Independently of the occupied site, the Nd average electron distribution maps show a pronounced anisotropy in the direction of the hexagonal conduction pathways. Finally, a shortening of the c axis and a narrowing of the conduction slabs have been observed to occur after ion-exchanged reactions. A schematic picture of the conduction region with possible neodymium sites obtained from the above-mentioned investigation methods is shown in Fig. 1(a).

The optical[6–8] and EPR (Ref. 7) spectra are consistent with Nd ions located in distorted octahedral mO(9d) positions. This suggested model indicates that the observed spectroscopic features may be explained in terms of large dislocations of O(5) oxygens and neodymium ions far away from sites with inversion symmetry.

X-ray-absorption spectroscopy (XAS) provides different information with respect to XRD: the lattice distortion around the incorporated ions in crystalline materials can be studied by a local point of view, while XRD gives only an average long range lattice structure. For example, in the case of solid solutions, significant differences were found between the average lattice structure refined by XRD and the local environment obtained by XAS of incorporated ions.[12]

Only a few papers have been published on the extended x-ray-absorption fine structure (EXAFS) of crystalline Nd-exchanged β''-alumina. The first EXAFS measurements of a 35% Nd-exchanged β''-alumina single crystal at the Nd L_3 edge showed a polarization dependence of the EXAFS signal, but the very low signal-to-noise ratio did not allow the authors to come to any definitive conclusion.[9]

A more recent work[11] was devoted to the study of rare-earth-doped β''-alumina crystals by EXAFS and computer simulation techniques, i.e., static-lattice defect-energy calculations (SLDEC) and molecular dynamics (MD). The EXAFS signal at the Nd L_3 edge for Nd^{3+}-exchanged ($\geq$90 %) β''-alumina crystal was measured in

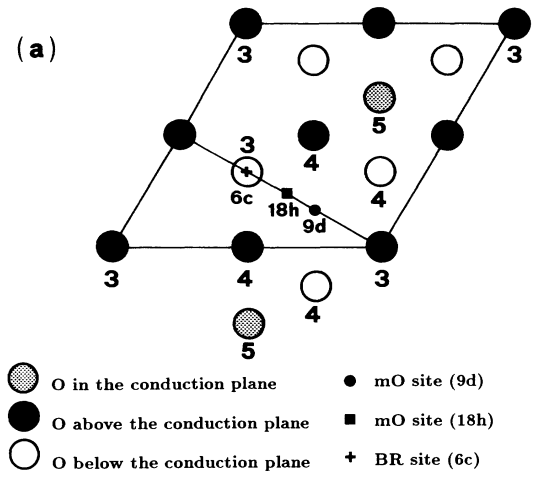

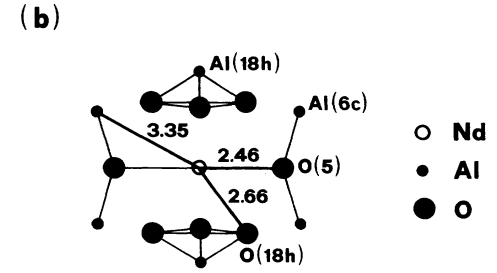

FIG. 1. (a) The conduction region of sodium β''-alumina. Circles indicate oxygen atoms located above, below, and in the conduction plane. The possible neodymium sites [mO(9d), mO(18h), and BR(6c)] are also shown. (b) The structural model of the Nd environment determined in this work: Neodymium is located in the distorted mO(9d) site.

transmission mode for a powdered sample. From cluster SLDEC calculations, it was found that the Nd(18h) site is the most stable, but also the mO(9d) site with highly symmetric arrangement of two nearest- and next-nearest-neighbor sodium vacancies is stable in a ~100% Nd-exchanged crystal. MD simulations of the 80% Nd-exchanged β''-alumina crystal, carried out for different temperatures (300, 600, and 1000 K), locate the Nd ions at BR sites, with a high probability of large vibrations towards positions midway between the BR and mO(9d) sites, i.e., to the mO(18h) site. The structural data obtained from EXAFS analysis as well as from computer simulations do not agree with the XRD data of Ref. 4 (see Table I). The authors' conclusion was that it is difficult to locate precisely the Nd ion on any one position from the available EXAFS data.[11]

An x-ray absorption near-edge structure (XANES) study[10] of the 40% Nd-exchanged β''-alumina crystal at the neodymium L_1 and L_3 edges has been also performed. The authors say that rare-earth ions are incorporated as trivalent ions, with high ionic bond, and remain essentially isolated and strongly localized in the β''-alumina matrix.

In this paper we present a detailed study of the Nd L_1- and L_3-edge XAS data for a powdered sodium β''-alumina crystals (60% of sodium content exchanged by Nd).

II. EXPERIMENTAL DETAILS

Single-crystal platelets of sodium β''-alumina, nominally $Na_{1.67}Mg_{0.67}Al_{10.33}O_{17}$, were grown by flux evaporation.[13] A 60% Nd^{3+}-exchanged crystal was obtained by keeping a platelet in molten $NdCl_3$ at 650 °C for 24 h. The extent of exchange was measured by a ^{22}Na radio-tracer diffusion technique.[14]

The sample for x-ray-absorption measurements was prepared as follows: The 60% Nd^{3+}-exchanged sodium β''-alumina crystal was finely ground and the powder was dispersed in methyl alcohol by an ultrasonic mixer and then uniformly deposited on a polytetrafluoroethylene membrane.

The x-ray-absorption spectra were measured in transmission mode at the ADONE storage ring (Frascati, Italy) using the EXAFS station on the PWA BX2S wiggler beam line. The electron energy was 1.5 GeV with current 10–40 mA. The synchrotron radiation was monochromatized using a Si(111) channel-cut crystal monochromator, and its intensity was measured by two ionization chambers containing krypton gas. The experimental spectra were recorded at room temperature in the energy ranges 6100–6700 eV at the Nd L_3 edge (E_{L_3}=6207.9 eV) and 7000–7300 eV at the Nd L_1 edge (E_{L_1}=7126.0 eV),[15] with an energy step 0.6–1.1 eV and an energy resolution equal to ~ 1 eV. Thus, the EXAFS

TABLE I. Summary of the structural data obtained from the analysis of the Nd L_3-edge EXAFS in this work. X-ray single-crystal diffraction (Ref. 4) and previous EXAFS results (Ref. 11) are also shown for comparison. (N is the number of atoms A located at a distance R from neodymium; σ^2 is the Debye-Waller factor.)

	EXAFS (present work) 60% exchanged			X-ray diffraction Ref. 4 100% exchanged		EXAFS Ref. 11 ≥90% exchanged		
A	N	R (Å)	σ^2 (Å^2)	N	R (Å)	N	R (Å)	σ^2 (Å^2)
O	2.3±0.5	2.46±0.02	0.001±0.001	2	2.460	4.08	2.342	0.018
O	5.1±0.5	2.66±0.04	0.025±0.010	4	2.758	3.21	2.537	0.029
O				2	2.781	3.79	2.820	0.009
Al	3.2±0.9	3.35±0.03	0.003±0.002			2.73	3.787	0.006
O	2.4±1.0	3.8±0.1	0.02±0.015			3.00	4.255	0.018

was analyzed only above the L_3 edge, and the XANES was studied at both edges. The range of the L_3 edge EXAFS is limited by the presence of the neodymium L_2 edge (E_{L_2}=6721.5 eV).

The crystalline $NdCoO_3$ and $NdNiO_3$ with the orthorhombic $GdFeO_3$ structure (distorted perovskite type) were used as reference compounds. Their XAS were recorded under the same conditions using a Si(220) channel-cut crystal monochromator.

III. RESULTS AND DISCUSSION

A. XANES

The near-edge region of the experimental x-ray-absorption spectra at the Nd L_1 and L_3 edges in Nd^{3+}-exchanged (60%) sodium β''-alumina is shown in Fig. 2. The comparison of our experimental data with Ref. 10 shows good agreement between XANES at both L_1 and L_3 edges both in the shape and in the amplitude of signals.

The Nd^{3+} ion has an electronic configuration $[Xe]4f^3 5d^0 6s^0$ with unoccupied $5d$ states and three $4f$ electrons that results in the specific behavior of L-edge XANES. The strong resonance shown by the L_3-edge spectrum is the so-called "white line" (WL), and it is attributed to the $2p \rightarrow \overline{5,\epsilon d}$ transition. In this process the final state of the photoelectron is the state in the continuum (ϵ) with $5d$ atomic character. The bar over $\overline{5,\epsilon d}$ indicates the excited state of the photoelectron in presence of a core hole at the $2p$ level screened by other electrons. The high intensity of the WL is due to the fact that the final state is well localized with a high density of $5d$ states.

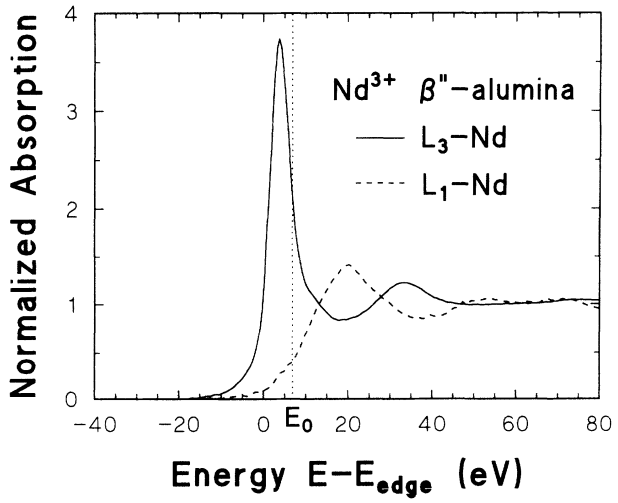

FIG. 2. Normalized experimental XANES spectra of the Nd L_1 and L_3 edges in Nd^{3+}-exchanged (60%) sodium β''-alumina crystal. E_{edge} is equal to 7126.0 and 6207.9 eV for L_1 and L_3 edges, respectively. The position of the photoelectron energy origin E_0, related to the continuum threshold, is shown by dotted line.

In contrast, no resonance in L_1-edge XANES is observed. To understand this fact, let us consider two main reasons for the possible origin of any remarkable feature at the L_1 edge.[16] The $2s \rightarrow \overline{5,\epsilon d}$ transition, which is forbidden in the dipole approximation, becomes allowed in the absence of the inversion center, e.g., in the case of tetrahedral symmetry. A shoulder can appear also when a distortion of local symmetry causes a hybridization of orbitals: In our case there is the possibility of a mixing of the $5d$ neodymium and $2p$ oxygen orbitals. The absence of any visible features at the Nd L_1 edge means that neodymium ions are located at sites with high symmetry.

The XANES region can be better understood when compounds such as NdF_3, Nd_2O_3, and NdF_3-BeF_2 glass are considered for the sake of comparison.[10,17] The WL intensity in Nd^{3+} β'' alumina is higher than in pure ionic NdF_3:[10] it was found[17] that the increase of the WL intensity both at Nd L_2 and L_3 edges is proportional to the covalency character of the chemical bond and therefore it can be attributed to the charge transfer from ligands to partly filled $4f$ orbitals of the Nd^{3+} ions. The existence of such an electron transfer mechanism in many neodymium-containing materials was previously proved by studying the $3d$ orbitals by photoelectron spectroscopy.[18] The reason for this process is that the $4f$ electrons in Nd^{3+} complexes are not completely localized and are involved in chemical bonding with ligands.[19,20] There is a significant covalent mixing between $4f$ shells of Nd^{3+} and valence shells of its ligands, which results in a non-negligible overlap of their wave functions. In particular, for Nd_2O_3 it was found that Nd $4f$ states mix with the O $2p$ orbitals giving a covalent contribution as large as ~17%.[19] Thus, in the case of the covalent bond, the additional electron back donated from ligands leads to an increase of screening effects of the photoelectron in a $5d$-like state which results in the localization of its wave function and in the increase of the matrix element (absorption or WL amplitude) with a $2p_{3/2}$ corelike initial state.

We can conclude that the Nd^{3+} ions in β'' alumina are located in high symmetry sites and are partly covalently bonded to neighboring oxygen ligands. This conclusion is also supported by the analysis of EXAFS data (see next section), which shows that strong bonding occurs mainly with two O(5) oxygens lying in the conduction plane. Our result does not agree with the statement of Ref. 10 that Nd ions are highly ionic and stay as isolated and highly localized ions in the β''-alumina matrix.

The maxima located in both L_1- and L_3-edge spectra above the continuum threshold E_0 shown in Fig. 2 correspond to the scattering resonances on the atoms of the first and outer coordination shells and are considered in the following section.

B. EXAFS

The experimental data were analyzed by the EXAFS data analysis software package EDA implementing the standard EXAFS data analysis procedure with slightly improved algorithms. A brief description of the analysis

procedure is given below.[21]

The x-ray-absorption coefficient $\mu(E) = \ln(I_0/I)$ was obtained from the intensities of synchrotron radiation, measured by two ionization chambers before (I_0) and after (I) the sample. The background contribution $\mu_b(E)$ was approximated by the Victoreen rule ($\mu_b = A/E^3 + B/E^4$) and subtracted from the experimental spectrum $\mu(E)$. Further, the atomiclike contribution $\mu_0(E)$ was calculated by a combined polynomial–cubic-spline technique in order to have a precise removal of the EXAFS signal zero line, and finally the EXAFS signal $\chi(E)$ was determined as $\chi(E) = (\mu - \mu_b - \mu_0)/\mu_0$ to convert $\chi(E)$ to a space of the photoelectron wave vector k, defined as $k = \sqrt{(2m/\hbar^2)(E - E_0)}$, where $(E - E_0)$ is the photoelectron kinetic energy measured from the inner core photoemission threshold (vacuum level). In the case of the L_3 edge of $5d$ elements, it is located behind the white line, which corresponds to the unoccupied $5d$ states. In the present work, the energy origin E_0 was located at 3.2 eV (which is the work function of Nd) above the white line maximum, according to the method earlier utilized by us.[22] Such a choice does not correspond exactly to the true position of the continuum threshold; however, it gives an error of ±0.5 eV which is sufficient for EXAFS analysis. The experimental EXAFS signal $\chi(k)$ was multiplied by a factor k^2 to compensate for the decrease of its amplitude with the increase of the wave vector value (see upper solid curve in Fig. 3).

The Fourier transform (FT) of the experimental EXAFS signal, with a Gaussian window in the range from 1.0 to 10.0 $Å^{-1}$, is shown in Fig. 4 (upper solid curve). There are two main peaks located at 2 and 3 Å and less intense peaks at 4 and 5.4 Å. The low intensity of the FT signal above 6 Å indicates that the noise in the experimental spectrum has "white" character (see Fig. 3). Finally, the absence of any significant contribution near $R = 0$ Å indicates good removal of the μ_0 signal. All FT's presented in this paper (except that of Fig. 7) are not corrected for the photoelectron phase shift; therefore the positions of peaks differ from the true crystallographic values. We note in Fig. 4 (upper solid line) the existence of a bump between 0.6 and 1.4 Å whose presence perturbs the first main peak and can lead to an incorrect determination of the structural parameters. Its origin is the oscillating behavior of the atomic cross section at the Nd L_3 edge. The importance of such an effect was previously pointed out in the case of arsenic and gaseous xenon,[23] but it is usually neglected in standard EXAFS analyses. Briefly, these oscillations are due to the photoelectron scattering in the outer regions of the absorbing atom (neodymium) potential which has an atomiclike character and occurs even in the absence of neighbors producing an EXAFS signal. This signal (see the dashed lines in Figs. 3 and 4) was calculated using the MSXAS code[24] and then subtracted from the experimental spectrum. The FT of the corrected experimental spectrum, shown in Fig. 4 as the lower solid curve, was used for the further analysis.

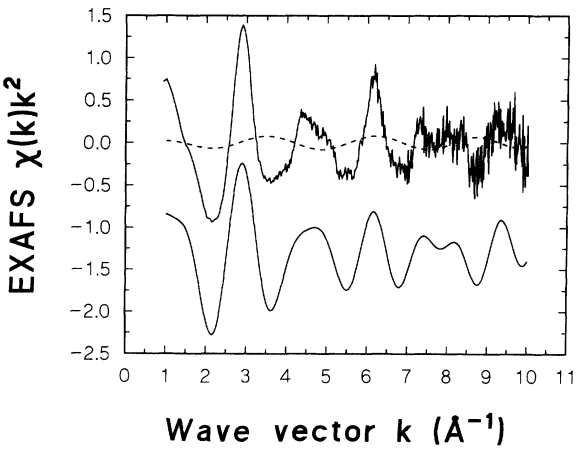

FIG. 3. Experimental EXAFS $\chi(k)k^2$ of the Nd L_3 edge (upper solid curve) and the contribution from the first two peaks (see Fig. 4) singled out by the back FT in the range 0.9–3.5 Å (lower solid line) after subtraction from the experimental spectrum of the oscillating part of the atomic cross section (dashed line).

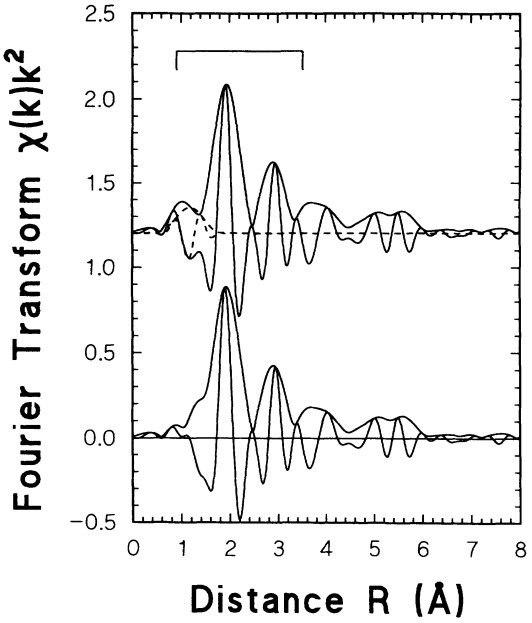

FIG. 4. Fourier transforms (FT) of the experimental spectrum before (upper solid curve) and after (lower solid curve) correction on the oscillating contribution from the atomic cross section whose FT is shown by dashed line. Both the modulus and imaginary parts of FT are shown. The range of the back FT is indicated (top solid line).

The contribution (solid curve in Fig. 3) to the total EXAFS signal from the first two highly visible peaks in Fig. 4 was singled out by a back FT in the range 0.9–3.5 Å. The estimated difference between signals derived from independent measurements was less than 6%. The EXAFS $\chi(k)k^2$ signal ($k = 1.0$–10.0 $Å^{-1}$) thus obtained was utilized in the best-fit multishell analysis procedure.

Calculations of the EXAFS function were based on the single-scattering curved-wave formalism[25] which is suitable for the first two peaks in the range 0.9–3.5 Å (Fig.

4). The EXAFS $\chi(k)$ was calculated using the expression

$$\chi(k) = \sum_i \frac{N_i}{kR_i^2} f_i(\pi, k, R_i) e^{-2\sigma_i^2 k^2} \times \sin[2kR_i + \phi_i(\pi, k, R_i)], \quad (1)$$

where N_i is the coordination number of the i shell, R_i is the radius of the i shell, σ_i is the Debye-Waller factor, $f_i(\pi, k, R_i)$ is the backscattering amplitude of the photoelectron by atoms of the i-coordination shell, and $\phi_i(\pi, k, R_i)$ is the phase shift of the photoelectron determined by central and scattering atoms. Backscattering amplitudes $f(\pi, k, R)$ and phases $\phi(\pi, k, R)$ were calculated by the FEFF3 code[26] for the Nd-O pair ($R = 2.5$ Å) and Nd-Al pair ($R = 3.5$ Å). Since the energy origin of the photoelectron, E_0, is defined in the FEFF3 code relative to the Fermi level E_F,[26] and our choice is the continuum threshold, $f(\pi, k, R)$ and phases $\phi(\pi, k, R)$ were corrected to have the energy reference as experimental EXAFS $\chi(k)$. Only transitions from the initial $2p_{3/2}$ state to final states with d character were considered, because the estimated contribution for the second allowed channel ($2p_{3/2} \rightarrow ns$) was less than 2.5% and it therefore may be neglected. The position of the energy origin of the photoelectron E_0 was fixed as described before, and the photoelectron mean free path contribution was automatically included in the scattering amplitude function by the use of the complex Hedin-Lundqvist (HL) exchange and correlation potential (ECP), based on the density functional formalism within the one-plasmon approximation, in the scattering T-matrix calculation.[27] Natural broadening was included through the core level width $\Gamma_{\text{core-hole}}$=3.5 eV (Ref. 28) (for the $2p_{3/2}$ level in the case of the Nd L_3 edge).

The importance of the multiple-scattering (MS) contribution was checked using the MSXAS code.[24] The obtained results show that the MS signals contribute above 3.5 Å in the FT.

The accuracy of the theoretical backscattering amplitudes and phases used in this work was verified using two reference materials $NdCoO_3$ and $NdNiO_3$. The

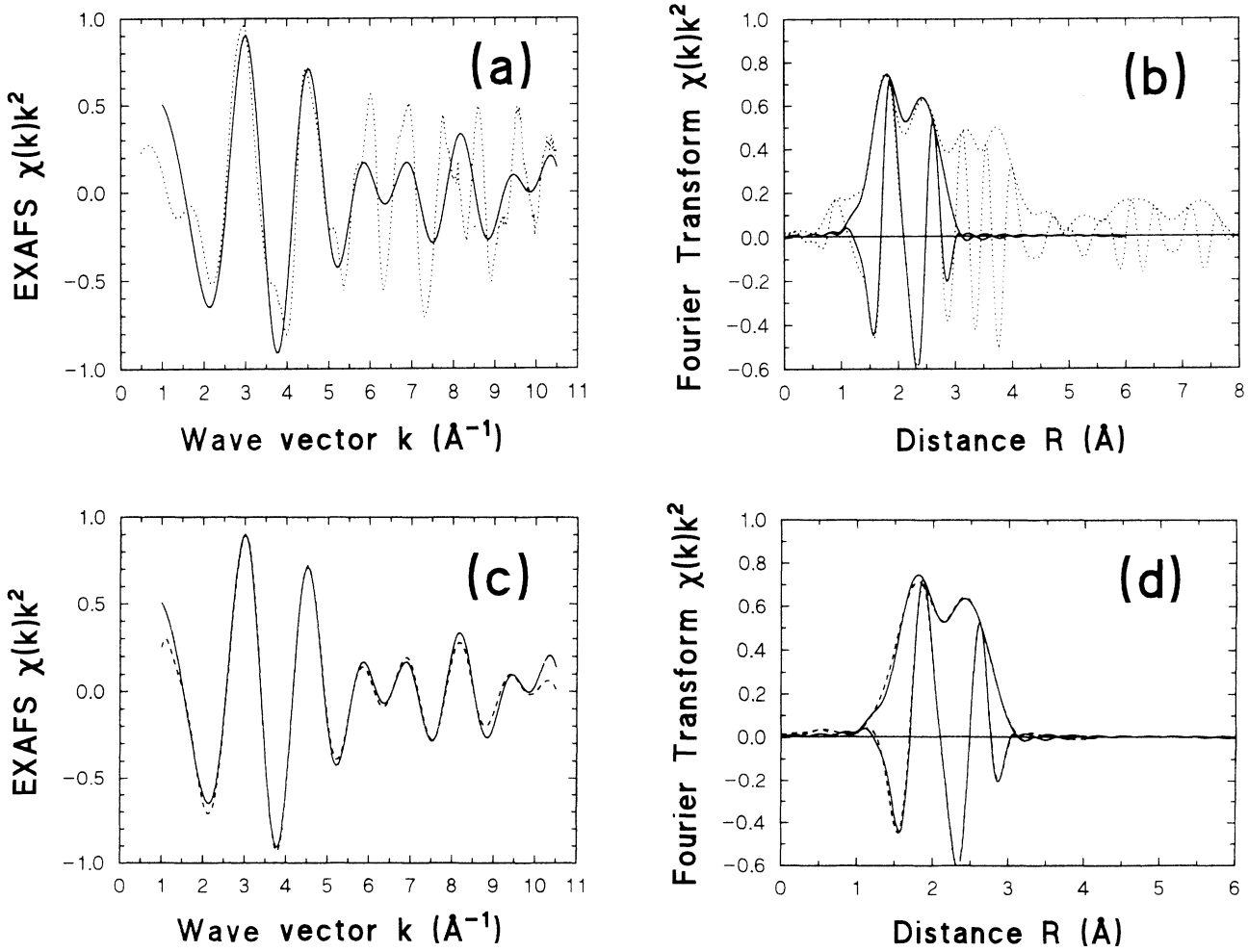

FIG. 5. (a) Experimental EXAFS $\chi(k)k^2$ of the Nd L_3-edge in $NdCoO_3$ (dotted line) and the contribution from the first two peaks [see (b)] singled out by the back FT (solid line). (b) Fourier transforms of spectra shown in (a). (c) The contribution from the first two peaks singled out by the back FT (solid line) and its best-fit four-shell model (dashed line). (d) Fourier transforms of spectra shown in (c).

EXAFS signals above the Nd L_3 edge for both crystals were extracted in the same way as previously described. The experimental and calculated spectra of the reference compounds are shown in Figs. 5 and 6. The results of the fitting procedure are presented in Table II. Note that the obtained crystallographic parameters are in good agreement with the x-ray and neutron powder diffraction data.[29,30]

At the first step of data analysis we tried to understand qualitatively the nature of the peaks in the FT. In Fig. 7 the modulus and imaginary part of FT's for the experimental EXAFS signal corrected for the calculated backscattering amplitude and phase of oxygen (upper curves) and aluminum (lower curves) are shown. In the first case, the maxima of the modulus and imaginary part coincide for the first peak at 2.5 Å and go in opposite phases for the second peak at 3.4 Å. In the second case, their behavior is opposite. Thus, we can conclude that the first peak has a predominant oxygen origin and the second one mainly an aluminum origin. Moreover, the approximate average distances are equal to R(Nd-O)=2.5 Å and R(Nd-Al)=3.4 Å. The asymmetry of the imaginary part relative to the maxima position indicates an asymmetric distribution of distances.

A more refined analysis was done using a best-fit procedure of the back FT EXAFS signal for the first two peaks using two-, three-, and four-shell models. The fit was done in the range from 1.5 to 9.0 $Å^{-1}$ to eliminate the influence of the back FT procedure at the beginning and end of the interval. The fitting parameters in all cases were coordination numbers, distances, and Debye-Waller factors. The maximum number of fitting parameters is limited in the general case by the number of independent data points, $N_{\mathrm{ind}} \approx 2\Delta k \Delta R/\pi$, where Δk and ΔR are respectively the widths in k and R space used in the fit.[31] In our case, N_{ind} is equal to 12.4 (Δk=7.5 and ΔR=2.6). Thus, if we take three fitting parameters per shell, the maximum number of shells which can be used is 4. In this work we used two-shell, three-shell, and four-shell models with respectively 6, 9, and 12 varying parameters. We tried to calculate all possible configurations of atoms within each model. One of the achieved best fit is

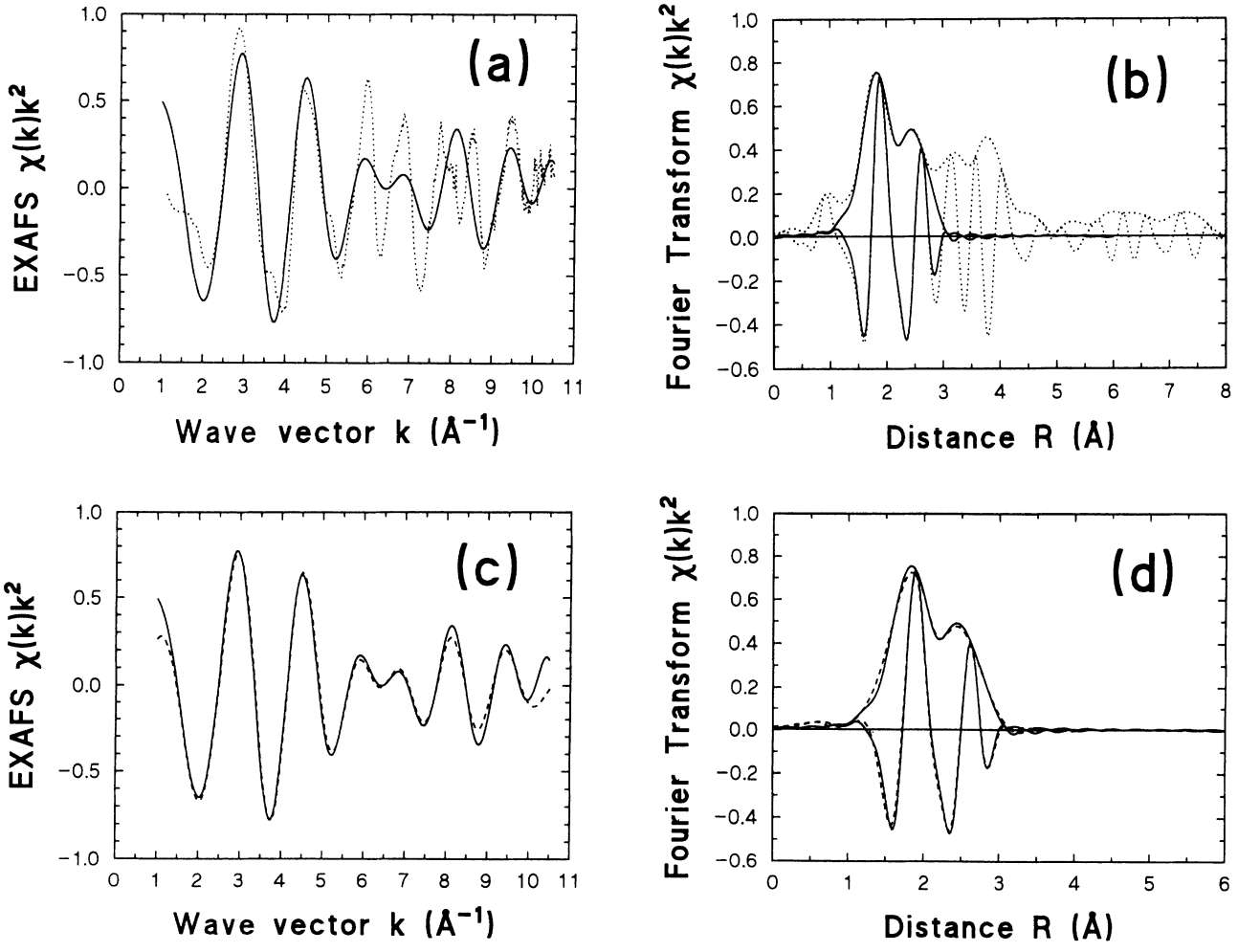

FIG. 6. (a) Experimental EXAFS $\chi(k)k^2$ of the Nd L_3 edge in $NdNiO_3$ (dotted line) and the contribution from the first two peaks [see (b)] singled out by the back FT (solid line). (b) Fourier transforms of spectra shown in (a). (c) The contribution from the first two peaks singled out by the back FT (solid line) and its best-fit four-shell model (dashed line). (d) Fourier transforms of spectra shown in (c).

TABLE II. Comparison of the best-fit structural data obtained from the EXAFS analysis with the x-ray and neutron powder diffraction data for $NdCoO_3$ (Ref. 29) and $NdNiO_3$ (Ref. 30) reference compounds. [N is the coordination number (±0.5); R is the Nd-O distance (±0.02 Å).]

	EXAFS		Diffraction	
Compound	N	R (Å)	N	R (Å)
$NdCoO_3$	2.7	2.38	2	2.35
	3.9	2.58	2	2.43
			3	2.61
	2.4	2.79	1	2.80
			2	2.95
	2.2	3.12	1	3.07
			1	3.15
$NdNiO_3$	2.4	2.40	3	2.37
	3.8	2.59	2	2.54
			2	2.64
	2.8	2.79	1	2.83
			1	2.95
	1.9	3.11	1	3.03
			2	3.15

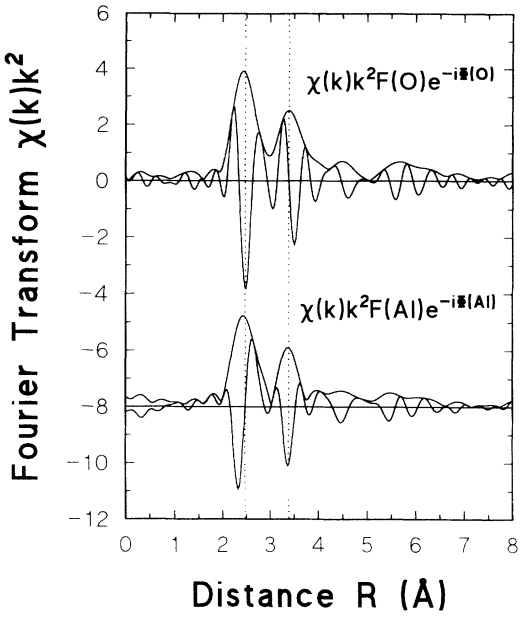

FIG. 7. Modulus and imaginary part of FT for the experimental EXAFS $\chi(k)k^2$ corrected on the backscattering phase and amplitude of oxygen (upper curves) and aluminum (lower curves). Dotted lines indicate the position of main peaks. Note the opposite behavior of the imaginary parts of FT in the two cases under the same peak.

presented in Table III. The fitting error was calculated by the expression

$$\text{error} = \frac{1}{m}\sum_{i=1}^{m}[\chi_{\text{model}}(k_i)k_i^2 - \chi_{\text{expt}}(k_i)k_i^2]^2, \qquad (2)$$

where m is the number of points. To examine the significance of adding a new shell to the EXAFS analysis, the method based on an F test was used.[32] The values of the left-hand side of the formula (11) of Ref. 32, for three- and four-shell models are presented in Table III. They both are larger than the value of the F function $F^5_{3,d} \simeq 2.7$ (we have chosen the significance level 5% and the number of points d was about 400). This means that the adding of the third and fourth shells is significant.

The result is shown in Fig. 8 in k and R space. Two shells of different atoms were found to produce the main contribution to the EXAFS signal: the group of oxygens at 2.46±0.02 Å and the group of aluminums at 3.35±0.03 Å. Their positions agree well with average distances previously obtained from the amplitude and phase corrected FT's. The two-shell model [dotted curve in Fig. 8(a)] allows one to approximate the general behavior of the EXAFS signal, but there is quite a large disagreement with experiment at high k values (7.5–9 $Å^{-1}$). To achieve better correspondence between theory and experiment, it is necessary to take into account two more shells. The addition of the second oxygen shell at 2.66±0.04 Å im-

TABLE III. Structural data obtained from the best-fit analysis of the Nd L_3-edge EXAFS and from the *rigid spinel-block* model calculated for the mO(9d) site. (N is the number of atoms A located at a distance R from the neodymium; σ^2 is the Debye-Waller factor.)

	EXAFS									mO(9d) site	
	Two-shell model			Three-shell model			Four-shell model				
A	N	R (Å)	σ^2 (Å^2)	N	R (Å)	σ^2 (Å^2)	N	R (Å)	σ^2 (Å^2)	N	R (Å)
O	5.9	2.52	0.016	2.9	2.46	0.0017	2.0	2.46	0.001	2	2.458
O				4.6	2.69	0.015	5.3	2.62	0.031	4	2.686
O										2	2.724
Al										2	3.068
Al	4.6	3.35	0.012	3.1	3.33	0.005	2.4	3.37	0.002	4	3.207
O							2.4	3.8	0.02	2	3.869
O										4	3.911
Error		9.3×10^{-3}			2.8×10^{-3}			1.7×10^{-3}			
F test					19.6			3.4			

proves the agreement of the first peak in the FT and the third oxygen shell at 3.8±0.1 Å improves the fit of the second peak. Thus, by using the four-shell model, it is possible to describe satisfactorily the shape of the experimental signal in the whole energy range from 1.5 to 9.0 $Å^{-1}$ [solid curve in Fig. 8(a)].

Here two remarks have to be made. First, one can see that the inclusion of an additional shell into the analysis does not influence strongly the distances obtained in the fit with a smaller number of shells. Second, it is necessary to point out that the contributions from the first three shells are very important to fit the experimental data and their parameters are stable relative to the starting values whereas the fourth shell of oxygens gives quite a small contribution to the experiment and its parameters are not well defined.

Table I contains a summary of the calculated parameters: the values are an average of different best-fit calculations, and the indicated errors are conservative estimates of possible uncertainties. The obtained coordination numbers and Debye-Waller (DW) factors are also presented. For the two nearest groups of oxygen atoms they agree very well with the crystallographic data (see Table III, last column). In the outer shells, their values are less precise, due to the lower sensitivity of the EXAFS technique to longer distances: the higher correlation with DW factors increases the estimated errors of coordination numbers. The very different values of the DW factors obtained for the first and third shells with respect to the second and fourth shells will be discussed in the following section, where a detailed comparison with XRD structural parameters is presented.

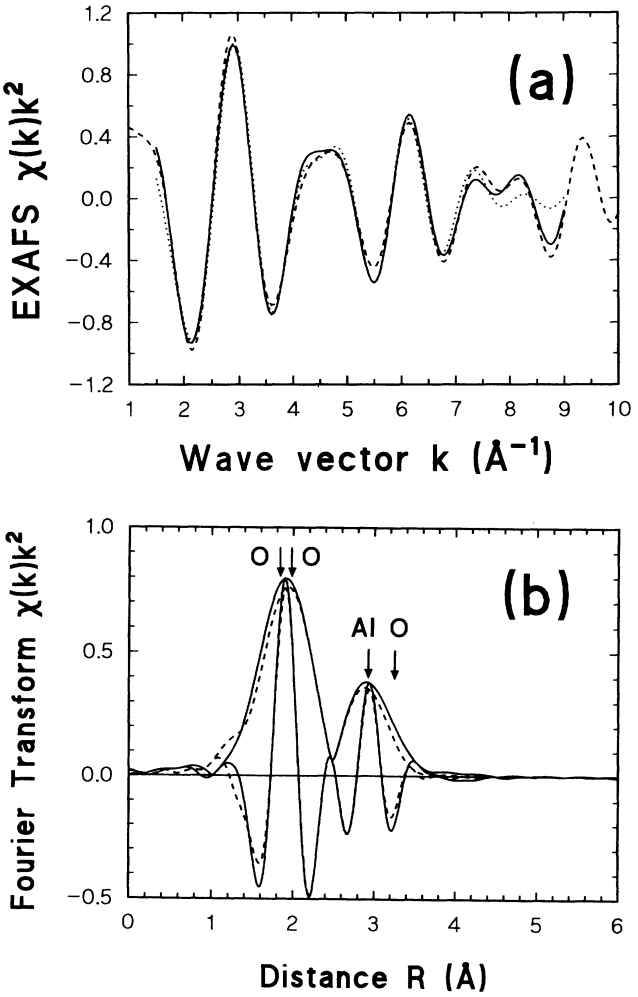

FIG. 8. (a) Experimental EXAFS $\chi(k)k^2$ of the Nd L_3 edge filtered out by the back FT in the range 1.2–3.5 Å(dashed line) and its best fit using two-shell (dotted line) and four-shell (solid line) models. (b) Fourier transform of the experimental spectrum shown in (a) (dashed line) and its best fit using the four-shell model (solid line). The positions of the oxygen and aluminum containing shells are indicated.

On the contrary, we must point out the significant difference with the previous EXAFS data of Ref. 11. In particular, in the previous EXAFS study, the nearest oxygens are placed at 0.1 Å shorter distances, and the outer shells of aluminum and oxygen positions are refined at 0.45 Å farther than in the present work. The authors of Ref. 11 do not discuss in detail the EXAFS data treatment procedure utilized in their work. In our opinion, the difference between the data from Ref. 11 and the present work is mainly due to a very different location of the E_0 position, which can lead to inaccuracies in the determination of interatomic distances. We are very confident in our results because in the present work (a) the experimental and calculated spectra have been referred to the same value of energy origin E_0, and thus it was not used as a fitting parameter, and (b) the accuracy of the used approach has been confirmed by its application to two reference materials.

C. Local structure of Nd ions

In the following, we will compare our results with the local structure around possible crystallographic sites of neodymium in β'' alumina. To compare the results obtained by EXAFS with crystallographic models, the radial distribution function (upper curve in Fig. 9) can be calculated according to the formula

$$g(r) = \sum_i (N_i/\sqrt{2\pi\sigma_i^2}) \exp[-(r - R_i)^2/(2\sigma_i^2)]. \quad (3)$$

This graphical representation is useful since it takes into account not only coordination numbers and peak positions but also Debye-Waller factor values.

The three main positions where the Nd ions may be located are mid-oxygen-site mO(9d), mid-oxygen-site mO(18h), and Beever-Ross-site BR(6c) [Fig. 1(a)]. Since the ion-exchange process changes the crystallographic structure of Na β''-alumina, we must model the local distortion. We have calculated the local structure parameters (coordination numbers and distances) for all three sites within two models using the lattice parameters from Ref. 4 (Table IV). In the first *rigid-spinel-block* model, we assumed that during the exchange process the starting c lattice parameter of Na β'' alumina (c=33.54 Å) (Ref. 1) decreases to the value in Nd-doped β'' alumina (c=33.2592 Å) (Ref. 4) due to the approaching of the

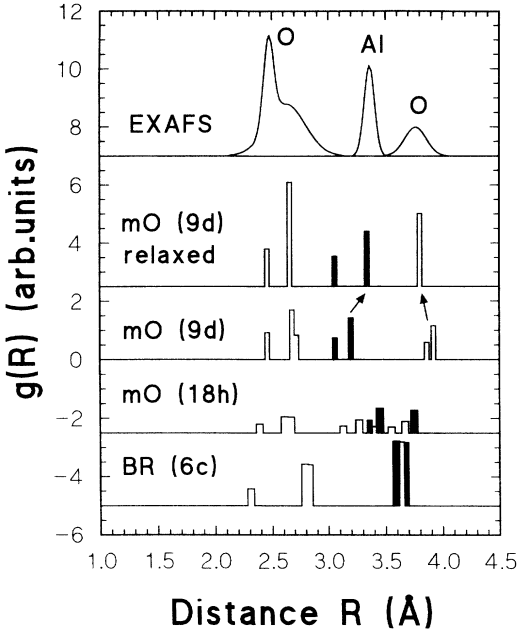

FIG. 9. Comparison of the radial distribution function (RDF) calculated from EXAFS data of this work using formula (4) with RDF's corresponding to BR(6c), mO(18h), and mO(9d) crystallographic sites (Table III) and the mO(9d) distorted site suggested in this work. The aluminum shells are shown in black. The arrows indicate the direction of shell shifts following the relaxation of the mO(9d) site.

spinel blocks without any change of their size: this leads to a narrowing of the conduction slab only. In the second *shrunken cell* model, we calculated the β''-alumina lattice from the refined positional coordinates taken from Ref. 4. As a result, we received a structure whose c lattice parameter decreases due to the global shrinking of all bonds. The set of distances thus obtained is presented in Table IV. The difference between these two models is not great from the local Nd-site point of view, especially if the error bars of the EXAFS data are considered, and it is much less than the difference between the local environment around the different mO(9d), mO(18h), and BR(6c) sites. The distribution of distances in the first shell is very wide in the case of the BR(6c) site: there are one short distance between neodymium and one oxygen located below the conduction plane and six long distances corresponding to oxygen atoms located in and above the plane (Fig. 9). It becomes narrower for the mO(18h) and mO(9d) sites, respectively. The second shell behaves oppositely: It is well defined in the case of the BR(6c) site, becomes very broadened for the mO(18h) site, and splits into two subshell for the mO(9d) site. In the last case the two subshells have a very well-defined origin: the first consists only of aluminum atoms and the second is formed only by oxygens.

The best agreement between the obtained radial distribution and structural models is achieved by slightly distorting the mO(9d) site: In this case only small shifts from crystallographic data (Fig. 9) of outer aluminum (Δ ~0.2 Å) and oxygen (Δ ~-0.1 Å) shells are necessary. For the mO(18h) site the agreement is worse because a shift of oxygen ions (Δ ~0.2 Å) in the first shell is required and the broadened distribution of distances above 3 Å is inconsistent with the well-defined shape of the second peak in the FT of the EXAFS signal. In the case of the BR(6c) site the disagreement becomes the largest. Here, it is necessary to distort all distances and, in addition, there is a big problem in the first coordination shell: the very short distance (~2.2–2.3 Å) is totally absent in the EXAFS signals. When one tries to improve the agreement by shifting the neodymium atom along the z axis (i.e., assuming the off-center position of neodymium) the four shortest distances become equal to ~2.46 Å, but the second contribution in the first coordination shell (oxygens at ~2.66 Å) disappears. A similar shift along the z axis in the case of mO(18h) or mO(9d) sites does not change their agreement with the obtained results. Besides the multishell best fit previously pre-

TABLE IV. Sets of distances calculated using the structural models of the neodymium environment in Nd^{3+}-exchanged β''-alumina crystal. The lattice parameters are $a = b = 5.628$ Å and c=33.259 Å.[4] (N is the number of atoms A located at a distance R from the neodymium.)

Rigid spinel-block model						*Shrunken cell model from Ref. 4*					
BR(6c) site		mO(18h) site		mO(9d) site		BR(6c) site		mO(18h) site		mO(9d) site	
N A	R (Å)	N A	R (Å)	N A	R (Å)	N A	R (Å)	N A	R (Å)	N A	R (Å)
1 O	2.187	1 O	2.257	2 O	2.458	1 O	2.308	1 O	2.375	2 O	2.458
3 O	2.675	2 O	2.566	4 O	2.686	3 O	2.774	2 O	2.594	4 O	2.761
3 O	2.828	2 O	2.594	2 O	2.724	3 O	2.828	2 O	2.668	2 O	2.782
6 Al	3.470	1 O	3.030	2 Al	3.068	6 Al	3.576	1 O	3.127	2 Al	3.142
6 O	3.542	2 O	3.181	4 Al	3.207	6 O	3.618	2 O	3.266	4 Al	3.266
6 Al	3.595	2 Al	3.250	2 O	3.869	6 Al	3.652	2 Al	3.359	2 O	3.920
		4 Al	3.380	4 O	3.911			1 O	3.390	4 O	3.963
		1 O	3.390					4 Al	3.441		
		2 O	3.592					1 O	3.544		
		4 Al	3.640					2 O	3.666		
		1 O	3.808					4 Al	3.743		

sented [with three free parameters (N, R, σ^2) in each shell], we performed some best fits starting from the selected crystallographic positions (see Table IV) mO(9d), mO(18h), and BR(6c) with fixed coordination numbers. Variations of distances were allowed within ±0.3 Å from their crystallographic values to simulate possible small distortions, and the Debye-Waller factors σ^2 were free parameters. The obtained results agree with previous conclusions: the mO(9d) site allows the best agreement with the smallest required distortions and the distortions in the case of the BR(6c) site are the largest. Thus, the mO(9d) site with two short (~2.46 Å) Nd-O bonds in the conduction region and about six Nd-O long bonds (with oxygens above and below the conduction region) seems preferable from the analysis of EXAFS data. This conclusion agrees qualitatively with the results of the XANES analysis suggesting that the Nd^{3+} ions in β''-alumina are located in high symmetry sites and partly covalently bonded to neighboring oxygen atoms.

Additional information can be obtained from the best-fitted values of the Debye-Waller factors. We must note that in such a complicated structure as β''-alumina, with a too short EXAFS spectrum (from 1.5 to 9.0 $Å^{-1}$), the absolute values of the Debye-Waller factors have more qualitative than quantitative character. Nevertheless, since the difference between the Debye-Waller factor values for the first and third shells and those for the second and fourth shells is about one order of magnitude, their relative values can be interpreted. There are two shells showing Debye-Waller factors significantly smaller than the others (Table I and Fig. 9): the first shell formed by two O(5) column oxygens linearly located at ~2.46 Å in the conduction plane and the third shell formed by four aluminum atoms located at ~3.35 Å in the spinel blocks above and below the O(5) bridging oxygens [Fig. 1(b)]. The small value of their Debye-Waller factors suggests that the thermal motion of oxygens at ~2.46 Å and aluminums at ~3.35 Å is highly correlated with that of neodymium. The second oxygen shell located at ~2.66 Å has a value of the Debye-Waller factor much greater than that of the previous two shells. This fact cannot be explained only by static disorder because two subshells at 2.69 and 2.72 Å (as suggested by XRD) give a contribution to the Debye-Waller factor of only about 0.001 $Å^2$, i.e., much smaller than the obtained value 0.025±0.010 $Å^2$. In contrast with the first case, the thermal vibration of these groups of oxygens seems to be uncorrelated with neodymium one. Temperature-dependent measurements are in progress in order to better study the influence of static and thermal disorder in the Debye-Waller factors, and to check our preliminary conclusion.

IV. SUMMARY

In this work we have presented a detailed analysis of the neodymium L_1- and L_3-edge x-ray-absorption spectra of a powdered 60% Nd-exchanged sodium β''-alumina crystal measured in transmission mode at room temperature.

The analysis of the XANES spectra shows that the Nd^{3+} ions are located at sites with high symmetry and they are partly covalently bonded to the neighboring oxygen ligands. Therefore, the presence of neodymium ions in positions near mO(9d) sites with eight oxygen neighbors seems to be more likely compared to BR(6c) sites with distorted fourfold coordination.

On the basis of the EXAFS spectra analysis we can propose the following model for the neodymium local environment in 60% exchanged sodium β''-alumina: most of the neodymium ions are located near the mO(9d) sites of the conduction region; they are strongly bonded to two O(5) oxygens which are located in the same plane and shifted from their ideal crystallographic positions in sodium β''-alumina crystal [Fig. 1(b)]. Thus, the Nd-O(5) distance becomes about 0.36 Å shorter. The shift of the O(5) atoms leads to a relaxation of the four aluminum Al(6c) atoms in the opposite way, so that the Nd-Al(6c) bond length becomes ~0.13 Å longer. The six oxygens located above and below the conduction region relax ~0.1 Å in the neodymium direction.

Comparative analysis of Debye-Waller factors suggests that the thermal motion of two oxygens O(5) and four aluminums Al(6c) can be correlated with that of neodymium, whereas there is no evidence of correlation between the neodymium and oxygens ions of the spinel blocks.

ACKNOWLEDGMENTS

The authors are indebted to Professor P.K. Davies (University of Pennsylvania) for kindly providing them with the crystal. They are also thankful to Dr. F. Tietz (Universität Hannover) for fruitful discussions and critical reading of the manuscript and Professor J. Garcia (Universidad de Zaragoza) for supplying specimens of reference compounds. A.K. and J.P. wish to thank Università di Trento, Consiglio Nazionale delle Ricerche, and Laboratori Nazionali di Frascati of the Istituto Nazionale di Fisica Nucleare for hospitality and financial support. They are especially grateful to the groups of Professor G. Dalba (Università di Trento) and Professor E. Burattini (Laboratori Nazionali di Frascati). This work has been partially supported by the Italian Consiglio Nazionale delle Ricerche under Contract No. 93-01312.CT02.

[1] J.P. Boilot, G. Collin, Ph. Colomban, and R. Comes, Phys. Rev. B **22**, 5912 (1980).
[2] G.C. Farrington, B. Dunn, and J.O. Thomas, Appl. Phys. A **32**, 159 (1983).
[3] M. Jansen, A.J. Alfrey, O.M. Stafsudd, D.L. Yang, B. Dunn, and G.C. Farrington, Opt. Lett. **9**, 119 (1984).
[4] W. Carrillo-Cabrera, J.O. Thomas, and G.C. Farrington, Solid State Ion. **28–30**, 317 (1988).
[5] P.K. Davies, A. Petford, and M. O'Keeffe, Solid State Ion. **18&19**, 624 (1986).

[6] A.J. Alfrey, O.M. Stafsudd, B. Dunn, and D.L. Yang, J. Chem. Phys. **88**, 707 (1988).
[7] B. Dunn, D.L. Yang, and D. Vivien, J. Solid State Chem. **73**, 235 (1988).
[8] H. Dai and O.M. Stafsudd, J. Phys. Chem. Solids **52**, 367 (1991).
[9] R. Wong, W.L. Roth, B. Dunn, and D.L. Yang, Solid State Ion. **18&19**, 599 (1986).
[10] M.L. den Boer, Y.S. Pak, K.J. Adamic, S.G. Greenbaum, M.C. Wintersgill, J.F. Lomax, J.J. Fontanella, B. Dunn, and G.C. Farrington, Phys. Rev. B **45**, 6369 (1992).
[11] T.S. Bush, C.R.A. Catlow, A.V. Chadwick, M. Cole, R.M. Geatches, G.N. Greaves, and S.M. Tomlinson, J. Mater. Chem. **2**, 309 (1992).
[12] T. Yokoyama, F. Takamatsu, K. Seki, K. Miyake, T. Tani, and T. Ohta, Jpn. J. Appl. Phys. **29**, L1486 (1990).
[13] J.L. Briant and G.C. Farrington, J. Solid State Chem. **33**, 385 (1980).
[14] R.B. Queeman, Ph.D. thesis, University of Pennsylvania, 1989.
[15] J.A. Bearden and A.F. Burr, Rev. Mod. Phys. **39**, 125 (1967).
[16] A. Balerna, E. Bernieri, E. Burattini, A. Kuzmin, A. Lusis, J. Purans, and P. Cikmach, Nucl. Instrum. Methods A **308**, 240 (1991).
[17] K.J. Rao, J. Wong, and M.J. Weber, J. Chem. Phys. **78**, 6228 (1983).
[18] H. Berthou, C.K. Jørgensen, and C. Bonnelle, Chem. Phys. Lett. **38**, 199 (1976).
[19] M.V. Ryzhkov, V.A. Gubanov, Yu.A. Teterin, and A.S. Baev, Z. Phys. B **59**, 1 (1985).
[20] S.P. Tandon and P.C. Mehta, J. Chem. Phys. **52**, 4896 (1970).
[21] A. Kuzmin, Ph.D. thesis, University of Latvia, 1992; A. Kuzmin and J. Purans, J. Phys. Condens. Matter **5**, 2333 (1993).
[22] A. Kuzmin, J. Purans, M. Benfatto, and C.R. Natoli, Phys. Rev. B **47**, 2480 (1993).
[23] B.W. Holland, J.B. Pendry, R.F. Pettifer, and J. Bordas, J. Phys. C **11**, 633 (1978). The modern theory of the oscillatory structure in the atomic background absorption has been recently developed and the effect has been found in many compounds [J.J. Rehr, C.H. Booth, F. Bridges, and S.I. Zabinsky (unpublished)]. Its amplitude seems to be higher in highly ionic compounds. The details of the calculations can be found in S.I. Zabinsky, Ph.D. thesis, University of Washington, 1993.
[24] M.F. Ruiz-Lopez, F. Bohr, A. Filipponi, A. Di Cicco, T.A. Tyson, M. Benfatto, and C.R. Natoli, in *X-Ray Absorption Fine Structure*, edited by S.S. Hasnain (Ellis Horwood, New York, 1991), pp. 75–77, and references therein; T.A. Tyson, Ph.D. thesis, Stanford University, 1991.
[25] W.L. Schaich, Phys. Rev. B **14**, 4420 (1976); S.J. Gurman, N. Binsted, and I. Ross, J. Phys. C **17**, 143 (1984).
[26] J.J. Rehr, J. Mustre de Leon, S.I. Zabinsky, and R.C. Albers, J. Am. Chem. Soc. **113**, 5135 (1991); J. Mustre de Leon, J.J. Rehr, S.I. Zabinsky, and R.C. Albers, Phys. Rev. B **44**, 4146 (1991).
[27] T.A. Tyson, K.O. Hodgson, C.R. Natoli, and M. Benfatto, Phys. Rev. B **46**, 5997 (1992).
[28] O. Keski-Rahkonen and M.O. Krause, At. Data Nucl. Data Tables **14**, 139 (1974).
[29] X. Liu and C.T. Prewitt, J. Phys. Chem. Solids **52**, 441 (1991).
[30] J.L. García-Muñoz, J. Rodríguez-Carvajal, P. Lacorre, and J.B. Torrance, Phys. Rev. B **46**, 4414 (1992).
[31] *X-Ray Absorption Fine Structure*, edited by S.S. Hasnain (Ellis Horwood, New York, 1991), pp. 751–770.
[32] R.W. Joyner, K.J. Martin, and P. Meehan, J. Phys. C **20**, 4005 (1987).

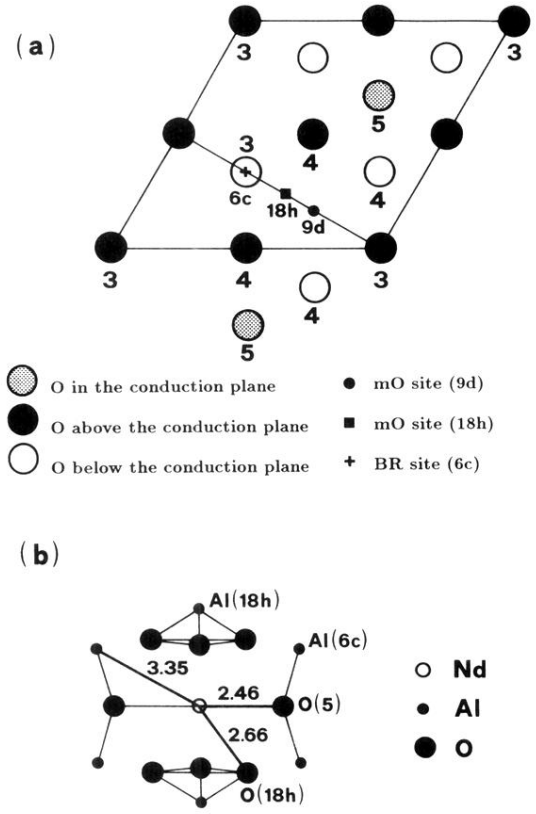

FIG. 1. (a) The conduction region of sodium β''-alumina. Circles indicate oxygen atoms located above, below, and in the conduction plane. The possible neodymium sites [mO(9d), mO(18h), and BR(6c)] are also shown. (b) The structural model of the Nd environment determined in this work: Neodymium is located in the distorted mO(9d) site.